Trapped Conformational States of Semiquinone (D + • Q B − •) Formed by B-Branch Electron Transfer at Low Temperature in Rhodobacter sphaeroides Reaction Centers †

ARTICLE *in* BIOCHEMISTRY · NOVEMBER 2006

Impact Factor: 3.02 · DOI: 10.1021/bi060854h · Source: PubMed

7 AUTHORS, INCLUDING:

Mark L Paddock
University of California, San Diego
107 PUBLICATIONS **3,339** CITATIONS
SEE PROFILE

Edward C Abresch
University of California, San Diego
55 PUBLICATIONS **1,896** CITATIONS
SEE PROFILE

Melvin Y Okamura
University of California, San Diego
132 PUBLICATIONS **7,729** CITATIONS
SEE PROFILE

Published in final edited form as:
Biochemistry. 2006 November 28; 45(47): 14032–14042.

Trapped Conformational States of Semiquinone ($D^{+\bullet}Q_B^{-\bullet}$) Formed by B-Branch Electron Transfer at Low Temperature in *Rhodobacter sphaeroides* Reaction Centers‡

M. L. Paddock*, **M. Flores**§, **R. Isaacson**, **C. Chang**, **E. C. Abresch**, **P. Selvaduray**, and **M.Y. Okamura**
Department of Physics, University of California, San Diego, La Jolla, CA 92093

Abstract

The reaction center (RC) from *Rhodobacter sphaeroides* captures light energy by electron transfer between quinones Q_A and Q_B, involving a conformational gating step. In this work, conformational states of $D^{+\bullet}Q_B^{-\bullet}$ were trapped (80K) and studied using EPR spectroscopy in mutant RCs that lack Q_A in which Q_B was reduced by the bacteriopheophytin along the B-branch. In mutant RCs frozen in the dark, a light induced EPR signal due to $D^{+\bullet}Q_B^{-\bullet}$ formed in 30% of the sample with low quantum yield (0.2%–20%) and decayed in 6 s. A small signal with similar characteristics was also observed in native RCs. In contrast, the EPR signal due to $D^+Q_B^-$ in mutant RCs illuminated while freezing formed in ~ 95% of the sample that did not decay ($\tau > 10^7$s) at 80K. In all samples, the observed *g*-values were the same (g=2.0026) indicating that all active $Q_B^{-\bullet}$ was located in a proximal conformation coupled with the non-heme Fe^{2+}. We propose that before electron transfer at 80K, the majority (~70%) of Q_B, structurally located in the distal site, cannot be stably reduced, while the minor (~30%) active configurations are in the proximal site. The large difference in the lifetimes of the un-relaxed and relaxed $D^{+\bullet}Q_B^{-\bullet}$ states is attributed to relaxation of protein residues and internal water molecules that stabilize $D^{+\bullet}Q_B^{-\bullet}$. These results demonstrate energetically significant conformational changes involved in stabilizing the $D^{+\bullet}Q_B^{-\bullet}$ state. The unrelaxed and relaxed states can be considered to be the initial and final states along the reaction coordinate for conformationally-gated electron transfer.

Keywords

Keywords: conformational gating; solvent relaxation; quinone movement; bacterial photosynthesis; electron transfer

Electron transfer reactions play crucial roles in many biological processes such as photosynthesis and respiration. In many cases the observed rate of electron transfer depends upon the electronic coupling and free energy differences according to Marcus theory (1). In other cases the observed rate of electron transfer is limited by another process such as conformational gating (2). Examples include protein motion (bc_1 complex), proton transfer, solvation changes or ligand binding steps that convert an inactive configuration of a protein to a state active in electron transfer (for review see ref 3). The electron transfer reaction, $Q_A^{-\bullet}Q_B \rightarrow Q_AQ_B^{-\bullet}$, between the quinone electron acceptors Q_A and Q_B in the bacterial

‡This work has been supported by the National Institutes of Health (Grant GM 41637).

*To whom correspondence should be addressed. Phone: (858)534-2504, Fax: (858)822-0007, E-mail: mpaddock@physics.ucsd.edu..
§Current affiliation: Max-Planck Institut für Bioanorganisch Chemie, Stiftstrasse 34-36, D-45470 Mühlheim an der Ruhr, Germany

Abbreviations: RC, reaction center; D, primary donor, dimer of bacteriochlorophylls; Q_A, primary quinone electron acceptor; Q_B, secondary quinone electron acceptor; $k_{AB}^{(1)}$, rate of *first* electron transfer *from* $Q_A^{-\bullet}$ to Q_B.

reaction center (RC) from *Rhodobacter (Rb.) sphaeroides* is an example of a gated electron transfer process. The reaction rate was shown to depend upon protein conformation based on changes of electron transfer upon freezing to cryogenic temperatures (4,5), crosslinking of the protein subunits (6) and embedding the protein in a glassy matrix (7) or PVA film (8). Furthermore, quinone (Q_A) substitution studies showed that the observed rate of electron transfer was independent of the driving force indicating a conformational gating mechanism (9). In this work we investigate the properties of different conformational states of the RC trapped by freezing the protein at cryogenic temperature. High energy states of $D^{+\bullet}Q_B^{-\bullet}$ were formed in a mutant RC (previously described in ref. 10) in which electron transfer to Q_B occurred *via* the low potential electron donor, bacteriopheophytin, by enhancing electron transfer along the B-branch of the RC (11,12). This allowed the high energy state(s) to be trapped at low temperature and the kinetic and spectroscopic properties to be measured.

The RC of the purple non-sulfur bacterium *Rb. sphaeroides* is the pigment protein complex responsible for the initial light induced electron transfer reactions that convert light energy into chemical energy (see *e.g.* 13,14). The cofactors in the RC are arranged in two parallel branches (designated A-branch and B-branch) across the protein (Fig. 1). Electron transfer normally occurs almost exclusively through the A branch from the primary donor, a bacteriochlorophyll dimer D, through monomeric bacteriochlorophyll (B_A), bacteriopheophytin (H_A) to ubiquinone (Q_A) in about 200ps followed by gated electron transfer to Q_B, the secondary quinone electron acceptor. The oxidized donor D^+ is reduced by a cytochrome c_2 molecule. Proton coupled electron transfer through the A-branch to Q_B utilizes two photons, two photoelectrons and two protons to form a quinol molecule Q_BH_2 within the pigment-protein RC complex (Eqn. 1) (see *e.g.* 18–20).

$$Q_B + 2hv + 2e^- + 2H^+ \rightarrow Q_BH_2 \quad (1)$$

where Q_BH_2 is the resultant quinol. The protons for this reaction are acquired from the cytoplasm. Following formation, the quinol can diffuse within the membrane to the cyt bc_1 complex where it is oxidized and the protons transferred to the periplasm. The electrons are shuttled between the cyt bc_1 complex and the RC by a mobile cyt c_2 electron carrier (see *e.g.* 14).

The reduction process of Q_B occurs in two sequential photo-induced electron transfer steps that result in electron transfer from a primary electron donor $Q_A^{-\bullet}$ to Q_B. The first electron transfer step, which is the focus of this work, occurs with an observed rate constant $k_{AB}^{(1)}$, which is in the time range 10^4–$10^5 s^{-1}$ (9,21,22). The kinetic decay is best described by the sum of several exponential components indicating that the reaction involves more than one step (22,23). The independence of the transfer rate on the driving force for electron transfer (9) has led to the proposal that the reaction is conformationally gated (for review see ref. 24).

An important functional feature of the RC is the position of Q_B. The location of quinone in the Q_B pocket is one of the least well determined parts of the RC crystal structure. This is in part due the function of Q_B as a mobile electron carrier. Early low resolution crystal structures showed Q_B to be relatively poorly defined (see *e.g.* 25). More recent high resolution structures show Q_B to be bound in two primary positions, a “distal” position in which the quinone head group is outside of the binding pocket and has only one H-bond to the protein (26,27) and a “proximal” position in which Q_B is bound by 4 H-bonds in the binding pocket (27,28) (see Fig. 1). These sites are ~5Å displaced. However, the preferred binding position is unclear. In different crystal structures the fraction of Q_B bound at the two sites varied from nearly all distal (26,27) to approximately 50% distal (28) to nearly all proximal (29). Furthermore, the preferred binding position may be a function of the cryoprotectant (if the crystal is frozen) and temperature (30). In contrast, $Q_B^{-\bullet}$, the reduced anionic semiquinone, has always been found

to be bound in the proximal site (27,28) consistent with the stabilization of the negative charge by H-bonds. This binding position is supported by EPR and ENDOR (31,32) and FTIR (33, 34) spectroscopic studies.

The x-ray crystal structure of the mutant RC used in this study, which includes the Ala-M260 → Trp mutation that displaces Q_A (described in more detail below), showed Q_B to be bound predominantly in the distal site (10). However, in the crystal structure of a mutant RC with only the single Ala-M260 → Trp mutation, McAuley *et al.* (16) reported that Q_B was bound at the proximal site. Thus, in RCs containing the Ala-M260 → Trp mutation Q_B has been observed in both the distal (10) and proximal (16) sites, as has been reported in the native RC.

The detailed interactions with the structure (conformation) of the surrounding protein are a major factor in determining the properties of Q_B. One well studied structural change is proton uptake induced by the formation of $Q_B^{-\bullet}$ (35,36). Located near the Q_B site are a number of acidic residues, including Asp L213, Glu L212 and Asp L210, that may change their protonation state upon quinone reduction. The changes in protonation state of the charged residues have been studied by computational methods (37,38) and infrared spectroscopy (39, 40). In addition to changes in protonation, the positions of nearby dipolar species will likely change in response to the charge introduced upon reduction. These include the positions of polar residues and bound water molecules around Q_B.

The different positions for Q_B observed in x-ray crystal structures led to the idea that the conformational gating step could be the movement of Q_B from the distal to the proximal site which involves a movement of ~5Å and a rotation of the head group along the isoprenoid tail. However, this is unlikely given the independence of the rate on the length of the isoprenoid chain of Q_B (9,41,42) and the observation of the same rate constant $k_{AB}^{(1)}$ measured in a mutant RC in which Q_B was predominantly structurally located in the proximal site (29). Another possible gating mechanism involves a conformational change in the protein that is required to favor the $Q_A^{-\bullet}Q_B \rightarrow Q_AQ_B^{-\bullet}$ reaction. In this case, the free energy is initially unfavorable, but becomes favorable due to a change in protein structure. This mechanism is supported by the observations of Li *et al.* (23) that replacement of Q_A with low potential quinones resulted in a fast component of electron transfer that was driving force dependent.

The present study was designed to examine changes in the environment of $Q_B^{-\bullet}$ that result from its reduction. The configurations of the protein before and after reduction were trapped by freezing RCs to cryogenic temperature as has been done previously (4,5). Since in the native RC $Q_B^{-\bullet}$ cannot be formed by electron transfer from $Q_A^{-\bullet}$ in samples frozen in the dark (5, 43), we developed a modified RC (Fig. 1) in which electron transfer to Q_B occurred through the B-branch bacteriopheophytin ($H_B^{-\bullet}$) (10,44–47) which has a much greater driving force for electron transfer (12). This allows higher energy states of $Q_B^{-\bullet}$ to become populated (47). To obtain significant electron transfer along the B-branch, we constructed a mutant RC that incorporated four mutations designed to increase the efficiency of B-branch electron transfer and a mutation Ala-M260 → Trp designed to remove Q_A (15,16). The mutations are: Leu-M214 → His (48), Gly-M203 → Asp (49–51), Tyr-M210 → Phe and Phe-L181 → Tyr (48, 52,53). The construction of this quintuple mutant was previously reported (10). In the quintuple mutant we could form $Q_B^{-\bullet}$ via B-branch electron transfer at room temperature (54) and in the frozen state (47) which allowed us to form and trap an intermediate state involved in the reduction of Q_B.

EPR spectroscopy was used to investigate the properties of the charge separated state $D^{+\bullet}Q_B^{-\bullet}$ in RCs frozen to cryogenic temperature (80K) either under illumination in which the protein is allowed to relax or frozen in the dark followed by illumination in which the protein is trapped in the initial un-relaxed configuration. The g-values of the EPR signals, the

dependence of the signal amplitude as a function of the light intensity and the lifetime of the charge separated states were measured. Since the protein may be present as an ensemble of states with different configurations, EPR measurements in the frozen state can serve to map out the distribution of protein conformational states. The lifetimes for charge recombination ($D^{+\bullet}Q_B^{-\bullet} \rightarrow DQ_B$) were used to assess the differences in the energies of the charge separated states formed by freezing in the dark or in the light which results in the formation of a stable $D^{+\bullet}Q_B^{-\bullet}$ state (54). A preliminary account of this work has been presented (47).

MATERIALS AND METHODS

Construction of the quintuple B-branch mutant RC

The mutations were incorporated as previously described (Paddock *et al.* 2001) with the following nucleic acid change(s): GCC → TGG (Ala-M260 → Trp), CTG → CAC (Leu-M214 → His), TAC → TTC (Tyr-M210 → Phe), GGT → GAC (Gly-M203 → Asp), TTC → TAC (Phe-L181 → Tyr). The RC proteins were isolated from semi-aerobically grown cells as described (55) with an optical ratio OR = A^{280}/A^{802} < 1.3. Q_B was reconstituted by adding a ~ 3-fold excess of UQ_{10} in 1%LDAO prior to dialysis against TMK (2mM Tris-HCl pH 8, 0.04 % β-D-maltoside, 5mM KCl).

EPR measurements

EPR spectroscopy (dχ"/dH *vs.* H) was performed at a microwave frequency of 9 GHz at T = 80 K as previously described (56). Two samples were made from the same RC material (~100μM RC). It was necessary to incubate the sample in 20–100μM ferricyanide/ferrocyanide to oxidize any $Q_B^{-\bullet}$ in the sample prior to illumination; in some *untreated* samples as much as 45% $Q_B^{-\bullet}$ was present prior to illumination. Once treated, one sample was frozen in liquid nitrogen in the dark. The other was illuminated by a projector (~1W/cm^2 white light, ~5 s) and frozen in liquid nitrogen under illumination. Upon illumination in the EPR cavity with a similar projector a charge separated signal was generated in the sample frozen in the dark (T=80K). The amplitude of this signal was measured as a function of the relative transmission of the actinic white light source. The transmission was decreased by using a series of neutral density filters. Upon turning off the exciting light, charge recombination was observed. The rate was measured by monitoring the time dependence of the signal at a fixed magnetic field value near B=3217G. The samples were stored in liquid nitrogen and reassessed ~ 1 year (10^7 s) later.

Model for fit of signal as a function of light intensity

Here we describe the model used to fit the dependence of the signal amplitude on the intensity of the actinic light. The basic equation is:

$$DQ_B \underset{k_{BD}}{\overset{k_{ex}}{\rightleftarrows}} D^{+\bullet}Q_B^{-\bullet} \quad (2)$$

where DQ_B is the RC in the ground state and $D^{+\bullet}Q_B^{-\bullet}$ is the RC in the excited charge separated state and k_{ex} and k_{BD} are the excitation and recombination rate constants, respectively. The rate of excitation is determined by the product of the quantum efficiency Φ_B and the rate of light absorption k_I. As the sample is excited with light (starting at time t=0), the $D^{+\bullet}Q_B^{-\bullet}$ state accumulates until the rate of recombination competes with the rate of excitation. When these two rates are equal, a steady state population is reached (*i.e.* no further changes in absorbance are observed). The steady state level of the change in absorption ($\Delta A^{865}{}_{ss}$) is determined by the ratio of the excitation to the sum of the excitation and recombination rate constants as shown in Eqn. 3.

$$\Delta A^{865}{}_{ss} = \Delta A^{865}{}_{max}\frac{k_{ex}}{k_{ex}+k_{BD}} = \Delta A^{865}{}_{max}\frac{\sigma I\Phi_B}{\sigma I\Phi_B + k_{BD}} = \Delta A^{865}{}_{max}\frac{1}{1+I_{1/2}/I} \quad (3)$$

where $\Delta A^{865}{}_{max}$ is the maximum change in absorption, and the rate of excitation is expressed as the product of the absorption cross section (σ), the light intensity (I), and the quantum efficiency (Φ_B). This equation describes a curve that increases linearly with increasing I when $\sigma I\Phi_B << k_{BD}$ but reaches a saturating value of $\Delta A^{865}{}_{max}$ when $\sigma I\Phi_B >> k_{BD}$. The value of I at half saturation, $I_{1/2}$, occurs at $k_{BD}/\sigma\Phi_B$. For some samples it was necessary to fit the data with the sum of two terms, each with its own values of $\Delta A^{865}{}_{max}$(i) and $I_{1/2}$(i) (Eqn. 3), where the (i) represents the values for the i^{th} sub-population; this is subject to the constraint that the sum of sub-populations is equal to the total, *i.e.* $\Delta A^{865}{}_{max}(total) = \sum_i \Delta A^{865}{}_{max}(i)$.

To estimate the quantum efficiency of the active population(s), we can compare the ratio of $I_{1/2}$ values assuming that the absorption cross sections are the same (Eqn. 4).

$$\Phi_B/\Phi_A = (k_{BD}/I_{B1/2}) * (I_{A1/2}/k_{AD}) \quad (4)$$

where Φ_B andΦ_A are the quantum efficiencies for forming $D^{+\bullet}Q_B^{-\bullet}$ and $D^{+\bullet}Q_A^{-\bullet}$, respectively, in the (sub)populations of the sample; k_{BD} and k_{AD} are the recombination rates of the $D^{+\bullet}Q_B^{-\bullet}$ and $D^{+\bullet}Q_A^{-\bullet}$ states, respectively; and $I_{B1/2}$ and $I_{A1/2}$ are the half saturation values for forming the $D^{+\bullet}Q_B^{-\bullet}$ and $D^{+\bullet}Q_A^{-\bullet}$ states, respectively. Since RC samples were made with similar RC concentrations, we expect the assumption that σ is the same between samples to introduce at most a systematic uncertainty of ~20%. This is much smaller than the relative differences discussed in this work and hence does not affect the conclusions.

RESULTS

EPR signals from mutant RCs frozen in the light and frozen in the dark

EPR spectroscopy was used to monitor the environment and lifetimes of the charge separated states formed in mutant RC samples frozen under illumination and frozen in the dark followed by illumination. In the Quintuple mutant sample frozen under illumination, the observed EPR signal had a *g*-value of 2.0026 and symmetric line-shape (see Frozen Light trace in Fig.2) that was characteristic of $D^{+\bullet}$ (57). The light frozen EPR signal did not decay at 80K ($\tau > 10^7$s). Upon illumination of the sample in the spectrometer, the signal amplitude was increased marginally (~5%) which is attributed to a minor fraction of RCs in the ground state prior to freezing.

The Quintuple mutant RC sample frozen in the dark had essentially no (< 1% of maximum) EPR signal (Frozen Dark trace, Fig. 2) following treatment with ferricyanide to remove any $Q^{-\bullet}$ in the stored sample (see Materials and Methods). However, upon illumination, an EPR signal (Frozen Dark + Light trace, Fig. 2) was generated that decayed (average τ = 6 s) when the illumination was terminated. The EPR signals seen in the quintuple mutant (Fig. 2) were not observed in samples to which the Q_B binding inhibitor stigmatellin was added, indicating that the electron transfer formed the $D^{+\bullet}Q_B^{-\bullet}$ state. The EPR spectra did not indicate the presence of a magnetically uncoupled semiquinone $Q_B^{-\bullet}$ which has an uncoupled *g*-value of 2.0053 (32). The uncoupled semiquinone would be expected to result in an observable shift in the *g*-value (2.0036) and introduce an asymmetry in the lineshape (1.5:1 ratio in relative amplitude of the peak and trough) (see *e.g.* 32). The absence of the uncoupled semiquinone indicates that the semiquinone spectrum is broadened by its interaction with the high spin Fe^{2+} (58).

Kinetics of Charge Separation and Recombination in Native and Quintuple mutant RCs

The kinetics of the formation and decay of the light induced $D^{+\bullet}$ EPR signals were studied by illumination of native and mutant RC samples frozen in the dark (T=80K) (Fig. 3). Following the light excitation, the EPR signals in Native and Quintuple mutant RCs decayed with different kinetics. Following the highest intensity illumination (I = 0.1 W/cm^2), the majority of the signal in the native RC (Fig. 3) decayed with τ = 30 ms, characteristic of decay from the $Q_A^{-\bullet}$ state ($D^{+\bullet}Q_A^{-\bullet} \rightarrow DQ_A$) (57,59). A minor component (see arrow Fig. 3) had a significantly slower decay with a $\tau \sim$ 6s. This lifetime was the same as measured in the Quintuple mutant (Fig. 3); a slightly better fit was obtained with two exponentials of equal amplitude with time constants τ of ~2s and ~10s, respectively (Fig. 4). The same kinetic decay was also observed in all other B-branch mutant RCs (Table 1). The *relative* fraction of the signal in the native RC that displayed slow kinetics was greater at low light intensity than at high light intensity (Fig. 3C) due to differences in the light saturation behavior of the fast and slow components (Fig. 5).

The lifetime of the charge separated state in 95% of the mutant samples frozen under illumination was > 10^7s (Fig. 4); the charge separated state has not decayed to the ground state in samples stored in liquid nitrogen. Thus, there is a dramatic >10^6-fold difference in the lifetimes of these samples.

Light saturation of Inducible Signal in Dark Frozen Sample at 80K

The amplitudes of the light inducible $D^{+\bullet}$ EPR signals from native and mutant RCs frozen in the dark were measured as a function of the light intensity (Fig. 5) to determine the saturating level of inducible signal. Equation 3 was fit to the measured data. For the mutant RCs, an adequate description of the observed amplitude as a function of light intensity required a minimum of two terms (Fig. 5). The need for fitting with multiple terms implies a heterogeneity of the sample, *i.e.* several sub-populations within the frozen sample.[#] In all mutant RCs, $D^{+\bullet}$ was formed in only a fraction (~30%) of the sample (Fig. 5).

In the single AWM260 mutant RC, the amplitude of the light inducible EPR signal as a function of light intensity could be fit with two terms in Eqn. 3 (see Table). The largest term that accounts for 70% of the sample describes the majority of the population in which stable charge separation was not formed. This is a consequence of $\sigma I\Phi_{B(1)} << k_{BD}$ for this population of the sample. The second term[‡‡] accounting for 30% of the sample describes the population in which the amplitude of the $D^{+\bullet}Q_B^{-\bullet}$ state increases with increasing light intensity. For this population, $\Phi_{B(2)} \sim 0.2\%$ using Eqn. 4 assuming that Φ_A = 100% at 80K (61). This is within uncertainty the same as the "overall" value of 0.4% observed at room temperature (10). The light saturation curves for the LHM214/AWM260 and GDM203/AWM260 were the same (Fig. 5b) indicating that within the resolution of this experiment the predominant effect is the AWM260 which eliminates the binding of Q_A (15,16).

To obtain an adequate fit of the light saturation curve of the Quintuple mutant RC (Fig. 5), a third term was included. The third term described a minor fraction (~20%) that had an apparently greater value for $\Phi_{B(3)}$ of ~20% (Table 2). Consequently the fraction of $\Phi_{B(2)}$ was observed to decrease to ~10% maintaining a value of ~30% for the sum of *all* active populations. Thus, the 30% active fraction appeared to be independent of the mutant system in which it was formed. The light saturation curves for the FYL181/LHM214/AWM260 was the same as the Quintuple, also requiring the third term with the larger $\Phi_{B(3)}$. Thus, the fraction with the larger $\Phi_{B(3)}$ is present in mutant RCs that contain the Phe-L181→Tyr replacement

[#]A heterogeneity of the illuminating light source would also result in the observed response. However, since this is not found for the native RC, we surmise that the effect is minimal and not the predominant reason for the observed heterogeneity.

[‡‡]This term likely represents the overall result of two or more sub-populations that are not clearly discriminated under the conditions of these measurements.

(FYL181). This enhancement of B-branch transfer was originally expected given the observed enhancement in mutant RCs of *Rb. capsulatus* (48,62), but was not observed in the room temperature measurements on the *Rb. sphaeroides* mutant RCs used in this study (10).

In the mutant RCs investigated in this study, the total active fraction of ~30% (extrapolated to infinite light intensity) was the same independent of the quantum efficiencies to form $Q_B^{-\bullet}$ (Fig. 5b). Thus, only a minor fraction of RCs can undergo stable charge separation at 80K while the majority cannot be trapped in a stable excited state.

For measurement made in the native RC (Fig. 5) one term was used to describe the observed behavior of the fast decaying phase and slow phases. The slowly decaying phase was found to attain half saturation at a lower light intensity than the fast phase. (Fig. 5) This was due to the slower rate of recombination that allowed the accumulation of the slowly decaying state despite its lower quantum efficiency for formation (Table 1). The apparent smaller amplitude compared to that observed in the mutant RC is a consequence of competition with formation of $D^{+\bullet}Q_A^{-\bullet}$. A more detailed description and analysis of the light induced signals observed in the native RC are presented in Paddock *et al* (60).

DISCUSSION

In this work, we investigated the electron transfer kinetics and EPR spectra of RC conformations trapped at low temperature both preceding and following Q_B reduction. In the frozen state, light induced electron transfer to Q_B in mutant RCs lacking Q_A was attributed to B-branch electron transfer similar to the reaction observed at room temperature (10,15). The lifetime of the $D^{+\bullet}Q_B^{-\bullet}$ state formed by freezing under illumination (after electron transfer) was $>10^6$-fold longer than that for RCs frozen in the dark (before electron transfer). This change is attributed to differences in the RC conformations between the neutral and charge separated states. We discuss below the implications of these findings on the configurations of neutral Q_B and of $Q_B^{-\bullet}$ trapped at 80K. We present a simple model to explain the experimental measurements and discuss the functional properties of Q_B bound in different conformations.

Electron Transfer Rates of RC in different Conformational States

In this study, electron transfer rates were measured for RCs frozen in different states at cryogenic temperature (5,43,63,64). The charge separated state $D^{+\bullet}Q_B^{-\bullet}$ that is formed in the mutant RCs by illumination during freezing represents a relaxed configuration and is characterized by a long lifetime ($\tau > 10^7$ s). Long lived $D^{+\bullet}Q_B^{-\bullet}$ states at low temperature were previously observed in native RC samples that were frozen under illumination. Using optical spectroscopy, Kleinfeld *et al* (5) observed that $D^{+\bullet}$ recovered slowly with distributed non-exponential kinetics. At 80K a significant fraction of $D^{+\bullet}$ had not recovered during the course of the experiment (10^4s). Xu *et al.* (43) observed recovery times of $D^{+\bullet}$ in the range of 10–100 s with a fraction that did not recover, attributed to samples that may have lost the electron on the acceptor side. Using EPR spectroscopy, Utshig *et al* (64) also observed a fraction that recovered non-exponentially in 10–100 s and a non-recovering fraction. The relative fraction that recovered depended on the illumination conditions during the freezing process. Since they were able to directly observe $Q_B^{-\bullet}$ using high-field EPR spectroscopy, they could rule out the possibility that the stability of the long lived state was due to loss of the electron from the acceptor $Q_B^{-\bullet}$. This long-lived fraction is analogous to that found in this study in the mutant RCs. The molecular basis for the long lifetime is currently under investigation. Preliminary ENDOR studies suggest that changes in the H-bond interactions of the RC with $Q_B^{-\bullet}$ provide additional stabilization to the relaxed $D^{+\bullet}Q_B^{-\bullet}$ state (65).

In dark frozen mutant RCs (*i.e.* frozen in the neutral ground state before electron transfer) the observed heterogeneity in the rates of electron transfer indicated a distribution of

conformational states. The major fraction (70%) of the sample was incapable in forming $D^{+\bullet}Q_B^{-\bullet}$ at cryogenic temperatures even at high light intensities (Table 1). This lack of activity could be due to either a slow rate of formation or a rapid decay of the excited state. The active fraction (~30%) formed $D^{+\bullet}Q_B^{-\bullet}$ upon illumination with a low quantum yield (Table 1) that was dependent on the mutations located at sites near the tetrapyrrole acceptor species. Irrespective of the quantum yield, the active fraction remained relatively constant (30%) indicating that it was determined by the properties near the Q_B site, which remain unchanged by the mutations (see below). In addition, the lifetime of the charge separated $D^+Q_B^-$ state was the same (τ =6 s) for all mutant RCs. (Table 1). Surprisingly, a small component of the EPR signal observed in the native RC had the same lifetime of 6 s (Fig. 3). The EPR signal showed a slowly rising component during illumination at lower intensities (Fig. 3) indicating a low quantum yield for formation (Table 1). Additional properties of this component led to its assignment to a small fraction of RCs that reduce Q_B *via* low efficiency B-branch electron transfer in the native RC (60). The identity of the 6 s time constants observed in RCs lacking Q_A and in the native RC indicates that the mutations have not altered the direct tunneling reaction between $D^{+\bullet}$ and $Q_B^{-\bullet}$. Thus, the environments around $D^{+\bullet}$ and $Q_B^{-\bullet}$ are substantially unchanged by B-branch mutations.

In previous studies, native RCs frozen under illumination displayed a distribution of lifetimes for the charge separated states ranging from 10s to > 10^4 s (5,43,64). In native RCs, reduction of Q_B occurs almost exclusively by electron transfer from $Q_A^{-\bullet}$. Since this transfer is fast and reversible, the electron hops between the two quinones during the freezing process. Thus, the protein structure surrounding Q_B may be affected by the details of competing processes such as protein relaxation, electron transfer, and freezing. Therefore, the native RC sample frozen under illumination may have structures intermediate between the relaxed structure and the un-relaxed structure. States with longer lifetimes would have structures that resemble the relaxed state. States with shorter lifetimes would have structures which resemble the un-relaxed state. This model qualitatively explains the distribution of lifetimes spanning many orders of magnitude. The distribution of rates is due to different protein conformational states that lie along the reaction coordinate leading from the neutral (DQ_B) in the un-relaxed state to the fully relaxed charge separated state ($D^{+\bullet}Q_B^{-\bullet}$) (5,43). The lifetimes measured in the present work on mutant RCs can be explained by this model. In dark-frozen (un-relaxed) mutant RCs the measured lifetime (τ ~6s) is shorter than the lifetimes measured in native RCs frozen under illumination (τ >10s) consistent with a totally un-relaxed state. In mutant RCs frozen in the light (relaxed) the long lifetime (τ >10^7s) is consistent with the lifetime of a totally relaxed state. The absence of Q_A eliminates electron hopping from $Q_B^{-\bullet}$ in these mutant RCs thereby constraining the RC to be in the $D^{+\bullet}Q_B^{-\bullet}$ state when illuminated during the freezing process. Thus, the conformational states found in the present study that are formed by freezing in the dark and in the light can be considered to be the initial and final states along the reaction path for electron transfer.

Molecular Basis for the Heterogeneity at the Quinone (Q_B) Binding Site

The data show that there are several distinct quinone (Q_B) states as well as distinct conformational states of the surrounding protein. In all mutant RCs, the total fraction of the sample that was activated in the dark frozen sample upon illumination was ~30%. The fraction was independent of the quantum efficiency of formation indicating that it is an intrinsic property of the acceptor (Q_B) site. Since the crystal structures of the RCs show two distinct binding positions (26–30), proximal and distal to the non-heme Fe^{2+}, the observed behavior likely reflects this distribution in the quinone binding positions. Below we discuss the rationale for assigning the different conformational states.

Conformational Assignments of the Q_B States in the Mutant RCs

The minor (~30%) active population capable of Q_B reduction in the sample frozen in the dark (un-relaxed conformation) is assigned to the fraction of RCs having a proximal Q_B ($D^{+\bullet}H_BQ_B^{-\bullet}(p)^U$) for the following reasons: (1) the relatively long lifetime of $Q_B^{-\bullet}$ indicates stabilization of $Q_B^{-\bullet}$ by H-bonds as is found in illuminated RC samples and crystals (27,28, 32), (2) there is no contribution of an uncoupled $Q_B^{-\bullet}$ EPR signal to the observed spectrum indicating a broadening of the s $Q_B^{-\bullet}$ signal due to its close proximity to the high spin Fe^{2+}, and (3) preliminary ENDOR spectroscopy indicated that the photochemically active Q_B is in the "proximal" site (65) (to be presented in further detail in a subsequent publication). Upon illumination at low temperature we form the charge separated state $D^{+\bullet}H_BQ_B^{-\bullet}(p)^U$ in RCs with proximal Q_B. The relatively rapid charge recombination time (τ =6 s) compared to the light frozen sample is due to the higher energy of this state due to the absence of stabilizing protein and solvent relaxation.[§§] These findings are in agreement with FTIR measurements made in frozen samples of a B-branch mutant, in which a similar minor fraction (~10%) of the dark frozen sample could undergo stable charge separation (66). The larger value of ~30% reported in this work is the hypothetical maximum fraction observed only at infinite light intensity.

The larger (70%) inactive population in RCs frozen in the dark is assigned to the fraction in the distal state $DH_BQ_B(d)$, based predominantly on the mutant crystal structure of the Quintuple RC in which the majority of Q_B is in the distal site (10). The lack of reactivity for the distal Q_B can be explained by a higher energy of the charge separated state due to lack of the strong H-bonds to both carbonyl oxygen atoms present in the proximal site. Alternatively, the lack of reactivity of the distal Q_B may result from a weaker electronic coupling to H_B. However the structural position of the quinone in the distal site is closer to H_B (10) which would be expected to increase the coupling (67,68). The relative occupancy of Q_B in the two binding sites in the frozen sample, *i.e* 3:1 for distal:proximal ratio, indicates only a modest difference in the binding energy (~1.5k_BT) between the two sites. Since binding to these two sites is nearly isoenergetic, small changes in the binding free energy resulting from temperature or external solvent could lead to a change in the relatively occupancy. This may be one reason for the reported differences in the binding position of Q_B (26–30,69) and the FTIR observation that Q_B prefers to bind at the proximal position at room temperature (46).

The conformation of RCs frozen in the light in the charge separated state is assigned to the proximal relaxed state $D^{+\bullet}H_BQ_B^{-\bullet}(p)^R$ in which solvent relaxation that stabilizes the charge separation has occurred. The EPR properties of this sample were similar to that of the light induced signals for $D^{+\bullet}H_BQ_B^{-\bullet}(p)^U$ discussed above. In addition, the larger signal from this sample allowed the observation of a broad g=1.82 signal (not shown) characteristic of the $Q_B^{-\bullet}Fe^{2+}$ coupled complex in native RCs (58). This indicates that $Q_B^{-\bullet}$ formed by B-branch electron transfer is located at the proximal site as it is in native RCs as shown by x-ray crystallography (27,28) and EPR and ENDOR spectroscopy (32). The protein response results in the dramatic >10^6-fold increase in the lifetime (stability) at 80K compared to the $D^{+\bullet}H_BQ_B^{-\bullet}(p)^U$ state.

Model for the Observed Kinetic Properties

The simplest model to explain the results (Fig. 6) assumes 4 possible RC configurations of the quinone in the protein. The quinone may be either in the distal (d) or proximal (p) position, and the protein in either an un-relaxed state (U) or a relaxed state (R) in which protein and solvent dipoles have oriented to stabilize the charge on $Q_B^{-\bullet}$. In the dark (ground state) sample,

[§§]To first order, we treat two $Q_B^{-\bullet}$ states as approximately the same since their recombination rates differ by ~4-fold, orders of magnitude less than the >10^6-fold difference observed between frozen in the light and frozen in the dark samples.

the majority (~ 70%) of the RCs are in the distal $DH_BQ_B(d)$ state that is photochemically inactive, *i.e.* stable charge separation does not occur. In the remaining ~30% of the RCs, Q_B is in the proximal position (see next section) where the RCs are photochemically active allowing the formation of the $D^{+\bullet}H_BQ_B^{-\bullet}(p)^U$ state. In the sample frozen under illumination, the states can interconvert prior to freezing resulting in the $D^{+\bullet}H_BQ_B^{-\bullet}(p)^R$ relaxed state. The relaxation lowers the energy of the charge separated state so that appreciable charge recombination does not occur at 80K. In the frozen state the different configurations cannot interconvert. Electron transfer that occurs in the dark frozen RC results in formation of the un-relaxed $D^{+\bullet}H_BQ_B^{-\bullet}(p)^U$ state with an average charge recombination rate $k_{BD}^U \cong 0.2\ s^{-1}$ (τ = 6s) that is $>10^6$ fold faster than that of the relaxed state $D^{+\bullet}H_BQ_B^{-\bullet}(p)^R$.

Functional Properties of Quinone (Q_B) Bound at the Different Sites

Of the four possible Q_B and protein configurations, only the states involving Q_B bound at the proximal site are observed (Fig. 6). Although the occupancy of the distal site, $DH_BQ_B(d)$, is significant at low temperature, stable charge separation to form the hypothetical $D^{+\bullet}H_BQ_B^{-\bullet}(d)^U$ state was not observed. This (lack of) observation indicates that $\sigma I \Phi_B << k_{BD}$, *i.e.* either its formation was unfavorable or its lifetime was not long enough to be observed. Likewise, the hypothetical $D^{+\bullet}H_BQ_B^{-}\mathbf{.(d)}^R$ state is less favored than $D^{+\bullet}H_BQ_B^{-\bullet}\mathbf{(p)}^R$ and is therefore also not observed. The change in the free energy of reduction of Q_B at the two different sites was estimated from electrostatic computations to be ~250meV higher than for quinone bound to the proximal site (70). This is consistent with our observations since the population of $D^{+\bullet}H_BQ_B^{-\bullet}(d)^R$ would be too small to observe.

One of the *active* Q_B states is $DH_BQ_B(p)^U$. Its corresponding charge separated state $D^{+\bullet}H_BQ_B^{-\bullet}(p)^U$ can be observed with an observed lifetime of ~6s ($k_{BD}^U \cong 0.2\ s^{-1}$). This charge separated state must have a free energy below that of $D^{+\bullet}H_B^{-}.Q_B(p)$ since its formation is favorable. The other *active* Q_B state is $D^{+\bullet}H_BQ_B^{-\bullet}(p)^R$ which had the greatest lifetime ($\tau > 10^7$s, 80K). The long lifetime is due to stabilization of the charge separated state *via* the protein response. At 80K the protein response is "frozen" in the sample resulting in the $> 10^7$s lifetime. Consequently, we did not observe the $DH_BQ_B(p)^R$ state in which the electron moves back to the oxidized donor. Long lived states were previously observed in both optical (5,43) and EPR spectroscopic studies (64).

The increased stability of the relaxed state compared to the un-relaxed state is not a consequence of a different binding position of $Q_B^{-\bullet}$ (see section above), therefore it is must be due to other changes, such as protonation and H-bonding. It has been proposed from electrostatic computations that the hydroxyl group of Ser-L223 reorients and forms a stabilizing H-bond to $Q_B^{-\bullet}$. Coupled to this reorientation is protonation (neutralization) of a nearby Asp-L213 (70–72). This proposal would be of sufficient free energy to account for the observed effects at 80K. We are in the process of experimentally investigating the molecular differences using ENDOR spectroscopy. The results of this study are the subject of a subsequent publication.

Conformational Gate

One of the remaining unknown steps related to RC function is the identification of the conformational gate that limits the observed rate for the first electron transfer. The existence of different protein conformations with very different characteristics was shown by the inhibition of electron transfer from $Q_A^{-\bullet}$ to Q_B in RCs frozen in the dark (4,5); this was in contrast to viable electron transfer in RCs frozen under illumination. Subsequently several studies to investigate these conformers (*i.e.* substates) were performed and the properties of charge separation investigated (43,73). These states have been proposed in a general sense to differ in the detailed interactions between Q_B and the protein. Electrostatic interactions have been shown to be of functional importance. In response to charge separation, amino acid groups

change their states of protonation resulting in a net proton uptake (35,36). The different protonation states are one contribution to the relative energy of these substates (37,38,74). Although some of the molecular details have been proposed from computational work (38, 70,72), experimental testing and verification of the molecular interactions has just recently been initiated (65).

Our results are consistent with the simple model for the conformationally gated electron transfer presented in Eqn. 5.

$$Q_A^{-\bullet}Q_B(d) \rightleftharpoons Q_A^{-\bullet}Q_B(p) \xrightarrow{k_C} (Q_A^{-\bullet}Q_B) \xrightarrow{k_{et(1)}} (Q_AQ_B^{-\bullet}) \qquad k_{AB}^{(1)} \longrightarrow \qquad (5)$$

where k_C is the rate constant of the rate-limiting conformational gate (9), $k_{et(1)}$ is the intrinsic electron transfer rate constant, ($Q_A^{-\bullet}Q_B$) is the intermediate state and $Q_A^{-\bullet}Q_B$(d) and Q_A^{-}•Q_B(p) are the initial states with Q_B in the distal (d) or proximal (p) location, respectively. The energy of this intermediate state lies above the two initial states as well as the final ($Q_AQ_B^{-\bullet}$) state. In particular, our results show that $Q_B^{-\bullet}$(d) cannot be stably formed confirming the necessity for Q_B to move into the proximal position for stabilization (27). Furthermore, our results show that a significant protein response is required to stabilize ($Q_AQ_B^{-\bullet}$). Although our results do not imply that the movement of quinone from the distal to proximal sites is rate-limiting, they do support the idea that the movement to the proximal site is a necessary *prerequisite* for its stabilization (27).

The un-relaxed state $D^{+\bullet}H_BQ_B^{-\bullet}(p)^U$ (Fig. 5) trapped in this work is sufficiently high in energy that it is not accessible *via* electron transfer from $Q_A^{-\bullet}$, the physiological electron donor in the native RC. Thus, it is most likely that the structural changes that occur in the conformational gate step of electron transfer to form ($Q_AQ_B^{-\bullet}$) (Eqn. 5) also occur in forming the $D^{+\bullet}H_BQ_B^{-\bullet}(p)^R$ state. In other words, the molecular changes that occur during the conformational gate step are reflected in the structural differences between the initial $D^{+\bullet}H_BQ_B^{-\bullet}(p)^U$ state and the final relaxed state $D^{+\bullet}H_BQ_B^{-\bullet}(p)^R$ observed in this work. Therefore, we consider the determination of the molecular differences between $D^{+\bullet}H_BQ_B^{-\bullet}(p)^U$ and $D^{+\bullet}H_BQ_B^{-\bullet}(p)^R$ to be of fundamental importance in understanding the reaction mechanism and are using ENDOR spectroscopy to investigate these differences.

Acknowledgements

We thank George Feher for helpful discussions and the reviewers of this paper who made it better by their critical comments.

References

1. Marcus RA, Sutin N. Electron transfer in chemistry and biology. Biochim Biophys Acta 1985;811:265–322.
2. Hoffman BM, Ratner MA. Gated electron transfer: when are observed rates controlled by conformational interconversion? J Am Chem Soc 1987;109:6237–6242.
3. Sharp RE, Chapman SK. Mechanisms for regulating electron transfer in multi-centre redox proteins. Biochim Biophys Acta 1999;1432:143–158. [PubMed: 10407138]
4. Chamorovsky SK, Remennikov SM, Kononenko AA, Venediktov PS, Rubin AB. New experimental approach to the estimation of rate of electron transfer from the primary to secondary acceptors in the photosynthetic electron transport chain of purple bacteria. Biochim Biophys Acta 1976;430:62–70. [PubMed: 816385]

5. Kleinfeld D, Okamura MY, Feher G. Electron-transfer kinetics in photosynthetic reaction centers cooled to cryogenic temperatures in the charge-separated state: evidence for light-induced structural changes. Biochemistry 1984;23:5780–5786. [PubMed: 6395882]
6. Noks PP, Lukashev EP, Kononenko AA, Venediktov PS, Rubin AB. Possible role of macromolecular components in functioning of photosynthetic reaction centers of purple bacteria. Mol Biol 1977;11:835–842.
7. Francia F, Palazzo G, Mallardi A, Cordone L, Venturoli G. Residual water modulates Q_A^--to-Q_B electron transfer in bacterial reaction centers embedded in trehalose amorphous matrices. Biophys J 2003;85:2760–2775. [PubMed: 14507738]
8. Francia F, Giachini L, Palazzo G, Mallardi A, Boscherini F, Venturoli G. Electron transfer kinetics in photosynthetic reaction centers embedded in polyvinyl alcohol films. Bioelectrochemistry 2004;63:73–77. [PubMed: 15110251]
9. Graige MS, Feher G, Okamura MY. Conformation Gating of the Electron Transfer Reaction $Q_A^-.Q_B \rightarrow Q_A.Q_B^-$, in Bacterial Reaction Centers of *Rb. sphaeroides* Determined by a Driving Force Assay. Proc Natl Acad Sci USA 1998;95:11679–11684. [PubMed: 9751725]
10. Paddock ML, Chang C, Xu Q, Abresch EC, Axelrod HL, Feher G, Okamura MY. Quinone (QB) reduction by B-branch electron transfer in mutant bacterial reaction centers from *Rhodobacter sphaeroides*: quantum efficiency and X-ray structure. Biochemistry 2005;44:6920–6928. [PubMed: 15865437]
11. Heller BA, Holten D, Kirmaier C. Control of electron transfer between the L- and M-sides of photosynthetic reaction centers. Science 1995;269:940–945. [PubMed: 7638616]
12. Kirmaier C, Laible PD, Hanson DK, Holten D. B-side charge separation in bacterial photosynthetic reaction centers: nanosecond time scale electron transfer from H_B^- to Q_B. Biochemistry 2003;42:2016–2024. [PubMed: 12590589]
13. Blankenship, RE.; Madigan, MT.; Bauer, CE. Anoxygenic photosynthetic bacteria. 2. Dordrecht, The Netherlands: Kluwer Academic Publishers; 1995.
14. Blankenship, RE. Molecular mechanisms of photosynthesis. Blackwell Science Inc; London: 2002.
15. Ridge JP, van Brederode ME, Goodwin MG, van Grondelle R, Jones MR. Mutations that modify or exclude binding of the Q_A ubiquinone and carotenoid in the reaction center from Rhodobacter sphaeroides. Photosynthesis R 1999;59:9–26.
16. McAuley KE, Fyfe PK, Ridge JP, Cogdell RJ, Isaacs NW, Jones MR. Ubiquinone binding, ubiquinone exclusion, and detailed cofactor conformation in a mutant bacterial reaction center. Biochemistry 2000;39:15032–15043. [PubMed: 11106481]
17. Kirmaier C, Gaul D, DeBey R, Holten D, Schenck CC. Charge separation in a reaction center incorporating bacteriochlorophyll for photoactive bacteriopheophytin. Science 1991;251:922–927. [PubMed: 2000491]
18. Feher G, Allen JP, Okamura MY, Rees DC. Structure and function of bacterial photosynthetic reaction centers. Nature 1989;339:111–116.
19. Hoff AJ, Deisenhofer J. Photophysics of photosynthesis: structure and spectroscopy of reaction centers of purple bacteria. Phys Rep 1997;287:2–247.
20. Okamura MY, Feher G. Proton transfer in Reaction Centers from photosynthetic bacteria. Annu Rev Biochem 1992;61:861–896. [PubMed: 1323240]
21. Vermeglio A. Secondary electron transfer in reaction centers of *Rhodopseudomonas sphaeroides*. Out-of-phase periodicity of two for the formation of ubisemiquinone and fully reduced ubiquinone. Biochim Biophys Acta 1977;459:516–524. [PubMed: 300250]
22. Tiede DM, Vazquez J, Cordova J, Marone PA. Time-resolved electrochromism associated with the formation of quinone anions in the *Rhodobacter sphaeroides* R26 reaction center. Biochemistry 1996;35:10763–10775. [PubMed: 8718867]
23. Li J, Gilroy D, Tiede DM, Gunner MR. Kinetic phases in the electron transfer from $P^+Q_A^-$ Q_B to $P^+Q_AQ_B^-$ and the associated processes in *Rhodobacter sphaeroides* R-26 reaction centers. Biochemistry 1998;37:2818–2829. [PubMed: 9485433]
24. Mulkidjanian AY, Kozlova MA, Cherepanov DA. Ubiquinone reduction in the photosynthetic reaction centre of *Rhodobacter sphaeroides*: interplay between electron transfer, proton binding and flips of the quinone ring. Biochem Soc Trans 2005;33:845–850. [PubMed: 16042612]

25. Lancaster CR, Michel H. The coupling of light–induced electron transfer and proton uptake as derived from crystal structures of reaction centres from *Rhodopseudomonas viridis* modified at the binding site of the secondary quinone, Q_B. Structure 1997;5:1339–1359. [PubMed: 9351808]
26. Ermler U, Fritzsch G, Buchanan SK, Michel H. Structure of the photosynthetic reaction centre from *Rhodobacter sphaeroides* at 2.65 Å´ resolution: cofactors and protein-cofactor interactions. Structure 1994;2:925–936. [PubMed: 7866744]
27. Stowell MH, McPhillips TM, Rees DC, Soltis SM, Abresch E, Feher G. Light-induced structural changes in photosynthetic reaction center: implications for mechanism of electron-proton transfer. Science 1997;276:812–816. [PubMed: 9115209]
28. Fritzsch G, Koepke J, Diem R, Kuglstatter A, Baciou L. Charge separation induces conformational changes in the photosynthetic reaction centre of purple bacteria. Acta Crystallogr D 2002;58:1660–1663. [PubMed: 12351882]
29. Kuglstatter A, Ermler U, Michel H, Baciou L, Fritzsch G. X-ray structure analyses of photosynthetic reaction center variants from *Rhodobacter sphaeroides*: structural changes induced by point mutations at position L209 modulate electron and proton transfer. Biochemistry 2001;40:4253–4260. [PubMed: 11284681]
30. Pokkuluri PR, Laible PD, Crawford AE, Mayfield JF, Yousef MA, Ginell SL, Hanson DK, Schiffer M. Temperature and cryoprotectant influence secondary quinone binding position in bacterial reaction centers. FEBS Lett 2004;570:171–174. [PubMed: 15251460]
31. Isaacson, RA.; Abresch, EC.; Lendzian, F.; Boullais, C.; Paddock, ML.; Mioskowski, C.; Lubitz, W.; Feher, G. Asymmetry of the Binding Sites of $Q_A^{-\bullet}$ and $Q_B^{-\bullet}$ in Reaction Centers of Rb. sphaeroides Probed by Q-Band EPR with ^{13}C-Labeled Quinones. In The Reaction Center of Photosynthetic Bacteria, Structure and Dynamics. Michel-Beyerle, M-E., editor. Berlin: Springer; 1996. p. 353-367.
32. Lubitz W, Feher G. The Primary and Secondary Acceptors in Bacterial Photosynthesis: III Characterization of the Quinone Radicals Q_A^-. and Q_B^-. by EPR and ENDOR. Appl Magn Reson 1999;17:1–48.
33. Breton J, Wakeham MC, Fyfe PK, Jones MR, Nabedryk E. Characterization of the bonding interactions of Q(B) upon photoreduction via A-branch or B-branch electron transfer in mutant reaction centers from *Rhodobacter sphaeroides*. Biochim Biophys Acta 2004;1656:127–138. [PubMed: 15178474]
34. Brudler R, de Groot HJM, van Liemt WBS, Gast P, Hoff AJ, Lugtenburg J, Gerwert K. FTIR spectroscopy shows weak symmetric hydrogen bonding of the Q_B carbonyl groups in *Rhodobacter sphaeroides* R26 reaction centres. FEBS Lett 1995;370:88–92. [PubMed: 7649310]
35. McPherson PH, Okamura MY, Feher G. Light-Induced Proton Uptake by Photosynthetic Reaction Centers from *Rhodobacter sphaeroides* R-26, I. Protonation of the One-Electron States $D^+Q_A^-$, DQ_A^-, $D^+Q_AQ_B^-$, and $DQ_AQ_B^-$. Biochim Biophys Acta 1988;934:348–368.
36. Maroti P, Wraight CA. Flash-induced HI binding by bacterial photosynthetic reaction centers: influences of the redox states of the acceptor quinones and primary donor. Biochim Biophys Acta 1988;934:329–347.
37. Beroza P, Fredkin DR, Okamura MY, Feher G. Protonation of interacting residues in a protein by a Monte Carlo method: application to lysozyme and the photosynthetic reaction center of *Rhodobacter sphaeroides*. Proc Natl Acad Sci U S A 1995;88:5804–5808. [PubMed: 2062860]
38. Alexov EG, Gunner MR. Incorporating protein conformational flexibility into the calculation of pH-dependent protein properties. Biophys J 1997;72:2075–2093. [PubMed: 9129810]
39. Hienerwadel R, Grzybek S, Fogel C, Kreutz W, Okamura MY, Paddock ML, Breton J, Nabedryk E, Mäntele W. Protonation of Glu L212 following Q_B^-Formation in the Photosynthetic Reaction Center of Rhodobacter sphaeroides: Evidence from Time-Resolved Infrared Spectroscopy. Biochemistry 1995;34:2832–2843. [PubMed: 7893696]
40. Nabedryk E, Breton J, Hienerwadel R, Fogel C, Mäntele W, Paddock ML, Okamura MY. Fourier Transform Infrared Difference Spectroscopy of Secondary Quinone Acceptor Photoreduction in Proton Transfer Mutants of. Rhodobacter sphaeroides Biochemistry 1995;34:14722–14732.
41. McComb JC, Stein RR, Wraight CA. Investigations on the influence of headgroup substitution and isoprene side-chain length in the function of primary and secondary quinones of bacterial reaction centers. Biochim Biophys Acta 1990;1015:156–171. [PubMed: 2404516]

42. Xu Q, Baciou L, Sebban P, Gunner MR. Exploring the energy landscape for Q(A)(−) to Q(B) electron transfer in bacterial photosynthetic reaction centers: effect of substrate position and tail length on the conformational gating step. Biochemistry 2002;41:10021–10025. [PubMed: 12146966]
43. Xu Q, Gunner MR. Trapping conformational intermediate states in the reaction center protein from photosynthetic bacteria. Biochemistry 2001;40:3232–3241. [PubMed: 11258940]
44. Laible PD, Kirmaier C, Udawatte CS, Hofman SJ, Holten D, Hanson DK. Quinone reduction via secondary B-branch electron transfer in mutant bacterial reaction centers. Biochemistry 2003;18:1718–1730. [PubMed: 12578387]
45. Wakeham MC, Goodwin MG, McKibbin C, Jones MR. Photo-accumulation of the $P^{+}Q_{B}^{-}$ radical pair state in purple bacterial reaction centres that lack the Q_A ubiquinone. FEBS Lett 2003;540:234–240. [PubMed: 12681514]
46. Breton J. Absence of large-scale displacement of quinone Q_B in bacterial photosynthetic reaction centers. Biochemistry 2004;43:3318–3326. [PubMed: 15035603]
47. Paddock, ML.; Flores, M.; Isaacson, RI.; Chang, C.; Abresch, EC.; Selvaduray, P.; Feher, G.; Okamura, MY. $Q_B^{-\bullet}$ Formation by B-Branch Electron Transfer in Reaction Centers from Rhodobacter sphaeroides in Photosynthesis: Fundamental Aspects to Global Perspectives. van der Est, A.; Bruce, D., editors. Allen Press; 2005b. p. 207-209.
48. Kirmaier C, He C, Holten D. Manipulating the Direction of Electron Transfer in the Bacterial Reaction Center by Swapping Phe for Tyr Near $BChl_M$ (L181) and Tyr for Phe Near $BChl_L$ (M208). Biochemistry 2001;40:12132–12139. [PubMed: 11580288]
49. Williams JC, Alden RG, Murchison HA, Peloquin JM, Woodbury NW, Allen JP. Effects of mutations near the bacteriochlorophylls in reaction centers from *Rhodobacter sphaeroides.* Biochemistry 1992;31:11029–11037. [PubMed: 1445841]
50. de Boer AL, Neerken S, de Wijn R, Permentier HP, Gast P, Vijgenboom E, Hoff AJ. High yield of B-branch electron transfer in a quadruple reaction center mutant of the photosynthetic bacterium Rhodobacter sphaeroides. Biochemistry 2002a;41:3081–3088. [PubMed: 11863447]
51. de Boer AL, Neerken S, de Wijn R, Permentier HP, Gast P, Vijgenboom E, Hoff AJ. B-branch electron transfer in reaction centers of Rhodobacter sphaeroides assessed with site-directed mutagenesis. Photosynth Res 2002b;71:221–239. [PubMed: 16228134]
52. Kirmaier C, Cua A, He C, Holten D, Bocian DF. Probing M-Branch Electron Transfer and Cofactor Environment in the Bacterial Photosynthetic Reaction Center by Addition of a Hydrogen Bond to the M-Side Bacteriopheophytin. J Phys Chem B 2002a;106:495–503.
53. Kirmaier C, Laible PD, Czarnecki K, Hata AN, Hanson DK, Bocian DF, Holten D. Comparison of M-Side Electron Transfer in *Rb. sphaeroides* and *Rb. capsulatus* Reaction Centers. J Phys Chem B 2002b;106:1799–1808.
54. Paddock ML, Isaacson R, Chang C, Feher G, Okamura MY. Conformations of Q_B^{-}. trapped by B side electron transfer in reaction centers from *Rhodobacter sphaeroides*. Biophys J 2004;86:11a.
55. Paddock ML, Rongey SH, Abresch EC, Feher G, Okamura MY. Reaction Centers from Three Herbicide Resistant Mutants of *Rhodobacter sphaeroides* 2.4.1: Sequence Analysis and Preliminary Characterization. Photosynth Res 1988;17:75–96.
56. Calvo R, Abresch EC, Bittl R, Feher G, Hofbauer W, Isaacson RA, Lubitz W, Okamura MY, Paddock ML. EPR Study of the Molecular and Electronic Stucture of the Semiquinone Biradical $Q_A^{-\bullet}$ QB $^{-\bullet}$ in Photosynthetic Reaction Centers from *Rb. sphaeroides*. Am Chem Soc 2000;122:7327.
57. McElroy JD, Feher G, Mauzerall DC. Characterization of primary reactants in bacterial photosynthesis. I. Comparison of the light-induced EPR signal (g = 2.0026) with that of a bacteriochlorophyll radical. Biochim Biophys Acta 1972;267:363–374. [PubMed: 4339582]
58. Butler WF, Calvo R, Fredkin DR, Isaacson RA, Okamura MY, Feher G. The electronic structure of Fe^{2+} in reaction centers from *Rhodopseudomonas sphaeroides* III. EPR measurements of the reduced acceptor complex. Biophysical J 1984;45:947–973.
59. Feher G, Isaacson RA, Ackerson LC, Okamura MY. On the question of the primary acceptor in bacterial photosynthesis: Manganese substituting for iron in reaction centers of *Rhodopseudomonas spheroides* R-26. Biochim Biophys Acta 1974;368:135–139. [PubMed: 4371037]

60. Paddock ML, Isaacson RA, Abresch EC, Okamura MY. Light induced EPR spectra of reaction centers from Rhodobacter sphaeroides at 80K: Evidence for reduction of Q_B by B-branch electron transfer in native reaction centers. Appl Magn Reson. 2006in press
61. Clayton RK, Yamamoto T. Photochemical quantum efficiency and absorption spectra of reaction centers from *Rhodopseudomonas sphaeroides* at low temperature. Photochem Photobiol 1976;26:67–70.
62. Chuang JI, Boxer SG, Holten D, Kirmaier C. High Yield of M-Side Electron Transfer in Mutants of *Rhodobacter capsulatus* Reaction Centers Lacking the L-Side Bacteriopheophytin. Biochemistry 2006;45:3845–3851. [PubMed: 16548512]
63. McMahon BH, Muller JD, Wraight CA, Nienhaus GU. Electron transfer and protein dynamics in the photosynthetic reaction center. Biophys J 1998;74:2567–2587. [PubMed: 9591682]
64. Utschig LM, Thurnauer MC, Tiede DM, Poluektov OG. Low-temperature interquinone electron transfer in photosynthetic reaction centers from Rhodobacter sphaeroides and Blastochloris viridis: characterization of Q(B)- states by high-frequency electron paramagnetic resonance (EPR) and electron-nuclear double resonance (ENDOR). Biochemistry 2005;44:14131–14142. [PubMed: 16245929]
65. Paddock ML, Flores M, Isaacson R, Chang C, Selvaduray P, Feher G, Okamura MY. Hydrogen Bond reorientation upon Q_B^-Formation Revealed by ENDOR Spectroscopy in Reaction Centers from. Rhodobacter sphaeroides Biophys J 2005;88:A204.
66. Wakeham MC, Breton J, Nabedryk E, Jones MR. Formation of a semiquinone at the Q_B site by A- or B-branch electron transfer in the reaction center from *Rhodobacter sphaeroides*. Biochemistry 2004;43:4755–4763. [PubMed: 15096044]
67. Noy D, Moser CC, Dutton PL. Design and engineering of photosynthetic light-harvesting and electron transfer using length, time, and energy scales. Biochim Biophys Acta 2006;1757:90–105. [PubMed: 16457774]
68. Tan ML, Balabin I, Onuchic JN. Dynamics of electron transfer pathways in cytochrome C oxidase. Biophys J 2004;86:1813–1819. [PubMed: 14990507]
69. Xu Q, Axelrod HL, Abresch EC, Paddock ML, Okamura MY, Feher G. X-ray structure determination of three mutants of the bacterial photosynthetic reaction centers from *Rb. sphaeroides*: Altered proton transfer pathways. Structure 2004;12:703–715. [PubMed: 15062092]
70. Zhu Z, Gunner MR. Energetics of quinone-dependent electron and proton transfers in *Rhodobacter sphaeroides* photosynthetic reaction centers. Biochemistry 2005;1:82–96. [PubMed: 15628848]
71. Alexov EG, Gunner MR. Calculated protein and proton motions coupled to electron transfer: electron transfer from $Q_A^-$to Q_B in bacterial photosynthetic reaction centers. Biochemistry 1999;38:8253–8270. [PubMed: 10387071]
72. Ishikita H, Knapp EW. Variation of Ser-L223 hydrogen bonding with the Q_B redox state in reaction centers from *Rhodobacter sphaeroides*, J. Am Chem Soc 2004;126:8059–8064.
73. Xu Q, Gunner MR. Exploring the energy profile of the Q(A)(−) to Q(B) electron transfer reaction in bacterial photosynthetic reaction centers: pH dependence of the conformational gating step. Biochemistry 2002;41:2694–2701. [PubMed: 11851416]
74. Grafton AK, Wheeler RA. Amino Acid Protonation States Determine Binding Sites of the Secondary Ubiquinone and Its Anion in the *Rhodobacter sphaeroides* Photosynthetic Reaction Center. J Phys Chem B 1999;103:5380–5387.

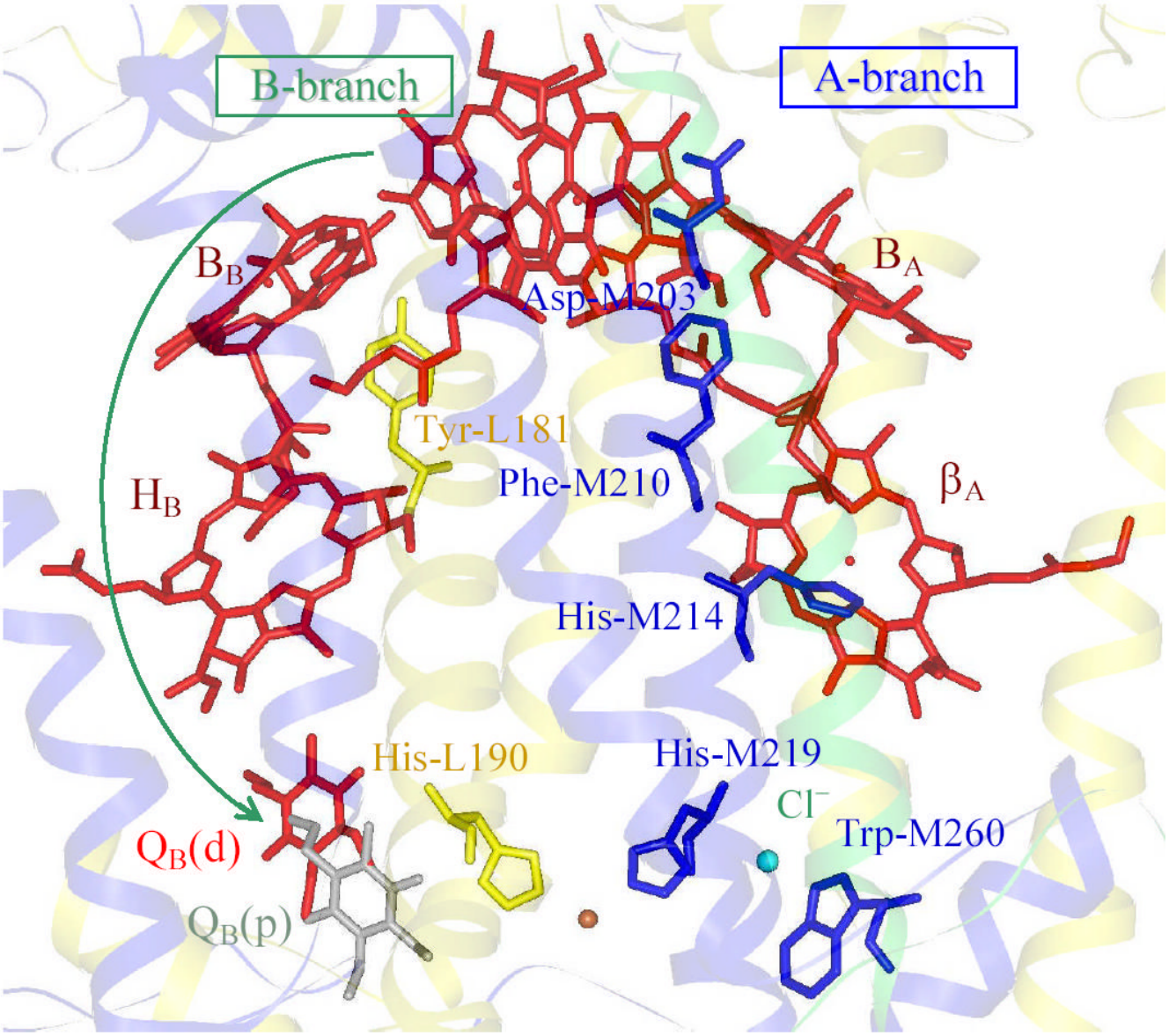

Figure 1.

Structure of the RC cofactors in the B-branch mutant used in this study (10) (PBD ID code 1YF6). Shown are the cofactors red imbedded in the backbone structure of the RC in light yellow (L subunit), blue (M subunit) and green (H subunit). Shown also are the Fe^{2+} ligands, His-M219 (yellow) and His-M230 (blue), and the five mutation sites – (1) Trp-M260 (15) and the consequential binding of a Cl^- anion displace the primary quinone electron acceptor, Q_A (16); (2) His-M214 results in the inclusion of a Mg^{2+} in the porphoryn ring creating β_A (17); (3) Tyr-M210; (4) Asp-M230; and (5) Tyr-L181 along the B-branch. These RCs have only one functionally active quinone electron acceptor located at the Q_B site. Q_B is bound at the distal (d) location and is hence labeled $Q_B(d)$. For reference, we show in green-grey the location of $Q_B^{-\bullet}$ in the native RC superimposed on the mutant structure; this quinone is located at the proximal (p) location and is labeled $Q_B(p)$. H_A and H_B are bacteriopheophytins, B_A and B_B

are bacteriochlorophylls and the subscript A or B refer to the cofactor binding to A-branch or B-branch, respectively.

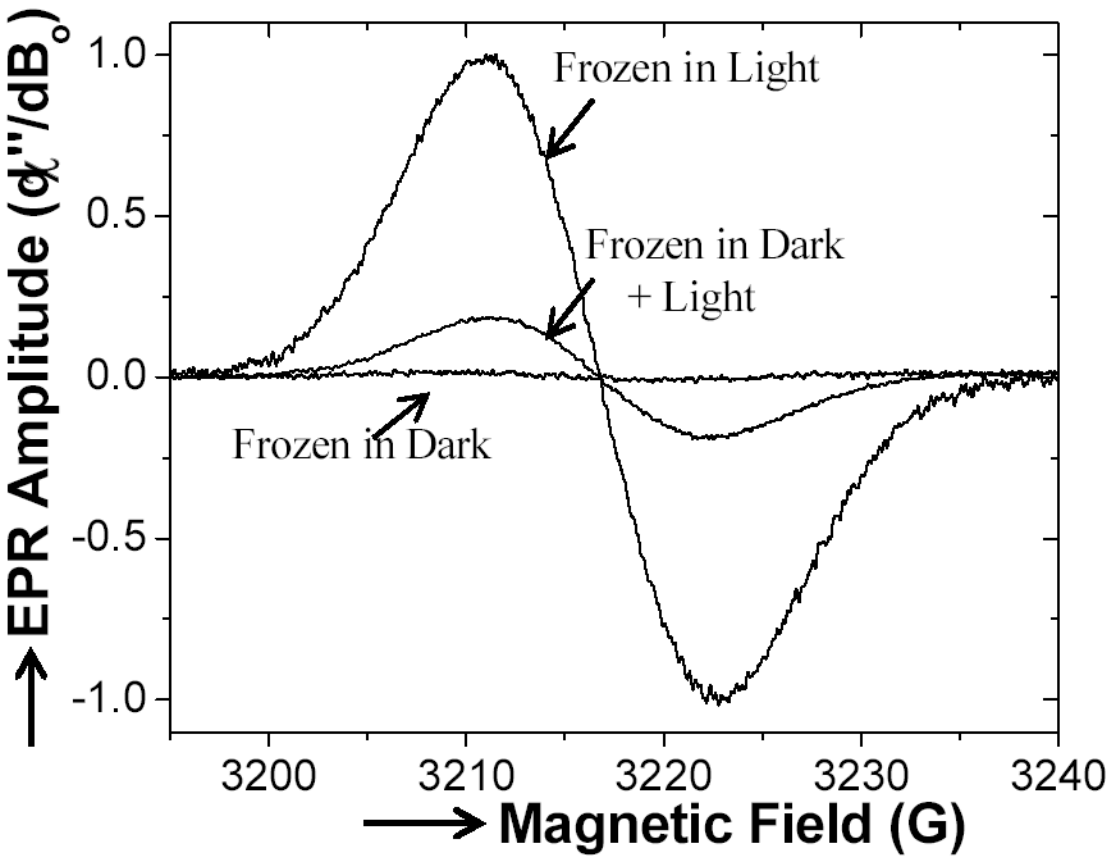

Figure 2.

EPR spectra (dχ''/dH) in the frozen state (T = 80K) of the B-branch mutant RC samples frozen either under illumination (Frozen in Light), frozen in the dark (Frozen in Dark) and illuminated in dark frozen sample (Frozen Dark + Light). The amplitude of the EPR signal of the dark frozen sample was ~20% of the amplitude of the sample frozen in the light indicating that a stable charge separation can be formed in a minor fraction of the sample. Note that both traces cross zero at the same value of the magnetic field showing that the *g*-values are the same in both samples and that the lineshapes (peak-to-trough ratios) are the same. Traces were normalized to the peak amplitude of the signal of the sample frozen under illumination. (Conditions: [RC] ~ 100μM, ID of EPR tube = 0.2cm, ν = 9GHz, 80K, 16 traces were averaged.)

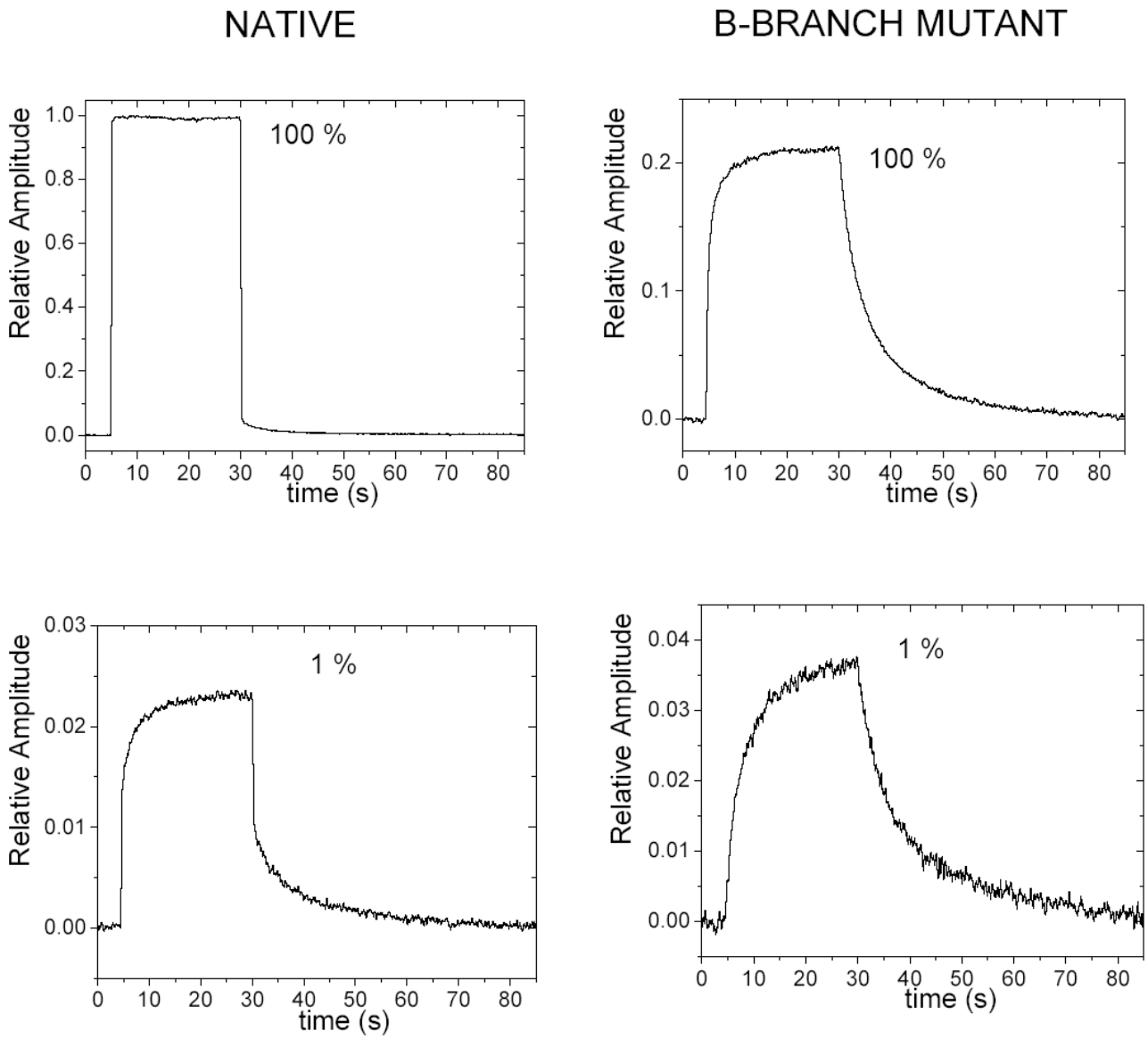

Figure 3.

EPR signal monitored before, during and following illumination of dark frozen samples for the native RC (left panels) and the Quintuple B-branch RCs (right panels). Shown on the top are the results of high light illumination (100%, maximum intensity) and on the bottom lower light illumination (1% of maximum intensity). Following illumination at high intensity (100%, I ~0.1W/cm^2), in the native RC the signal recovery is predominantly (95%) fast (τ = 30ms) with a small component of ~5% having a slower recovery time (τ = 6s). The faster recovery is indicative of the $D^{+\bullet}Q_A^{-\bullet} \rightarrow DQ_A$ reaction (57,59). The *relative* fraction of the signal with the slower recovery time is larger at lower illumination intensity (1%). In the mutant RC, the recovery of the EPR signal had no fast component and the decay time was the same as the slower phase observed in the native RC (τ = 6s). During illumination at lower intensity, the EPR signal had a slower rate of formation. This result indicates a low quantum efficiency process that is due to B-branch transfer in the mutant RC and has been attributed to B-branch

transfer in the native RC (60). All traces were normalized to the peak amplitude of the signal of the sample frozen under illumination. (Conditions: same as in Figure 2, magnetic field fixed at 3211 G, field modulation ΔH= 1 G, average of 10–100 traces.)

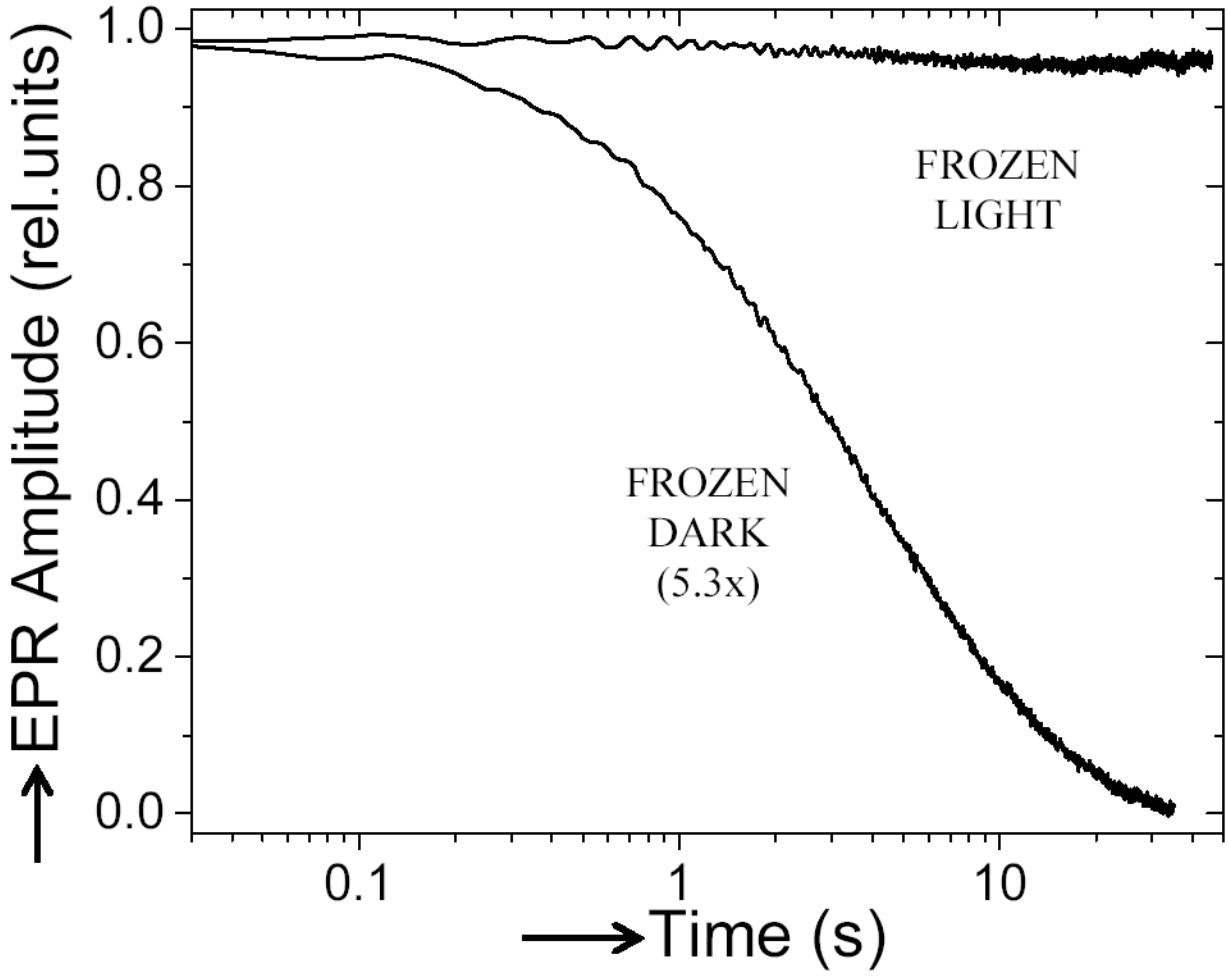

Figure 4.

Decay of the charge separated state in the B-branch mutant RC samples. Following illumination in the frozen state, the decays of the charge separated signals were monitored using EPR spectroscopy and plotted as a function of log time. In the dark frozen sample, the signal from the 20% of the sample in which charge separation was observed (see Figure 3) decayed with an average time constant of ~6 s (rate constant ~0.2 s^{-1}); a better fit of the decay is obtained with two phases of equal amplitude and time constants of 2s and 10s. In contrast, the charge separated state generated in the sample frozen under illumination was stable for > 10^7s. The amplitude of the signal from the frozen in the dark sample was increased 5.3-fold for a better comparison of the decay kinetics. (Conditions same as Fig. 2.)

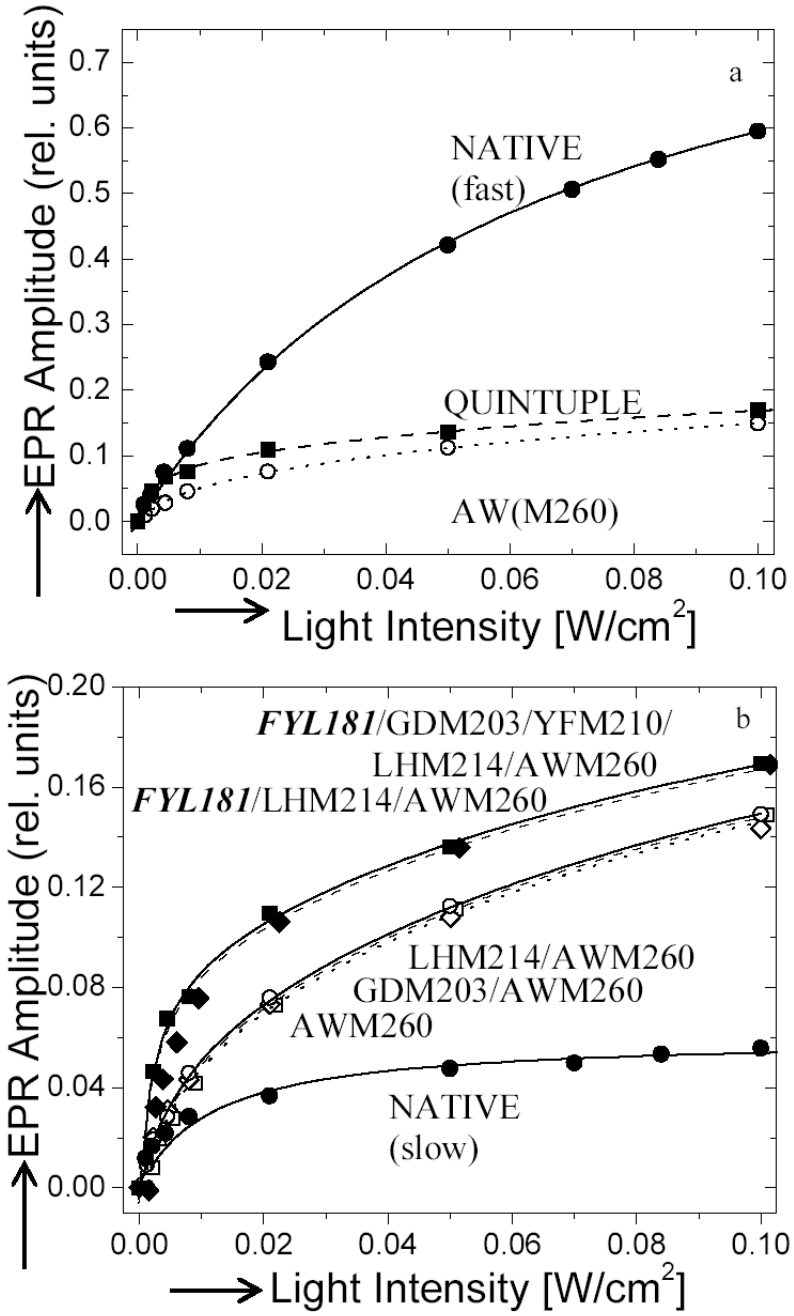

Figure 5.

Light saturation curve of the reversible inducible signal observed in the Frozen Dark + Light sample (Fig. 2). The EPR amplitude, normalized to that observed in the duplicate sample that was frozen under illumination, was measured as a function of the CW light intensity. (a) Shown is the comparison of the data for the native (•) and Quintuple (▪) and AWM260 (○) mutant RCs. The native data were fitted (solid lines) to a single term of Eqn. 3; the AWM260 to two terms; the Quintuple to three terms (see text). The maximum possible amplitude of the active population(s) was 1.0 (100%) in the native RC and ~30% in both mutant RCs. (b) Shown here is the comparison of different mutant RCs. The light intensity dependence can be fit with two terms for the AWM260 (○), GDM203/AWM260 (□) and LHM214/AWM260 (◊) mutant RCs.

A third term was required for the ***FYL181***/LHM214/AWM260 (♦) and ***FYL181***/GDM203/YFM210/LHM214/AWM260 (•) (Quintuple) RCs. This additional term was associated with the Phe-L181→Tyr mutation (***FYL181***) introduced along the B-branch. (Conditions same as Fig. 2.)

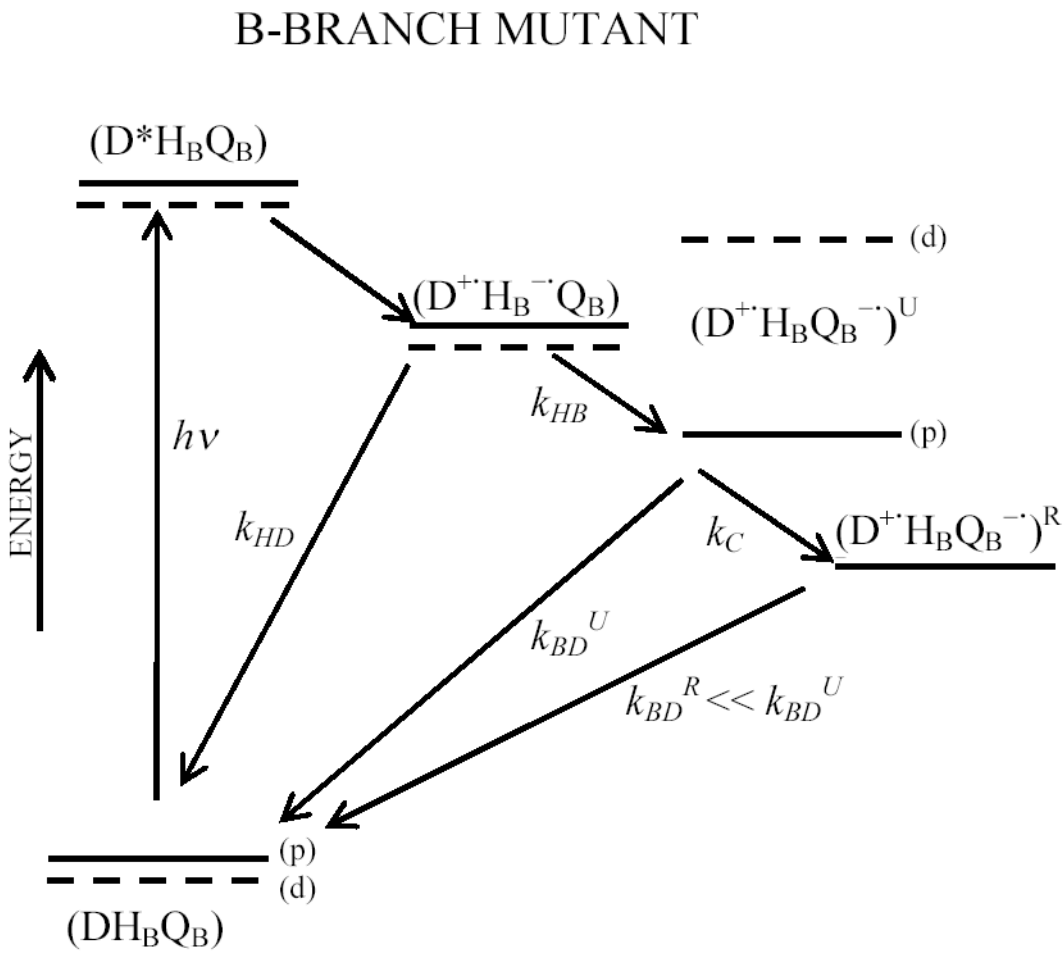

Figure 6.

Proposed energy level diagram of the ground and charge separated states consistent with the experimental results of this work. The DH_BQ_B is the ground state in one of two protein configurations with Q_B in either the "distal" (d) (dashed lines) or "proximal" (p) (solid lines) sites, respectively. $D^{+\bullet}H_BQ_B^{-\bullet}(p)^U$ and $D^{+\bullet}H_BQ_B^{-\bullet}(p)^R$ are the two observed charge separated states in which $Q_B^{-\bullet}$ is formed in the "proximal" site with the surrounding protein either in the un-relaxed (U) or the relaxed (R) configuration, respectively. k_{HD} and $k_{BD}{}^U$ are the recombination rate constants as indicated and k_C is the rate constant of the protein relaxation. Light excitation of the ground state resulting in the formation of $D^*H_BQ_B$ and electron transfer to form $D^{+\bullet}H_B^{-\bullet}Q_B$. In the dark frozen RCs, electron transfer occurs in a minor population to $Q_B(p)$ forming $D^{+\bullet}H_BQ_B^{-\bullet}(p)^U$ (Paddock *et al.* 2005b, subsequent publication). In contrast, electron transfer to $Q_B(d)$ is not observed suggesting that $D^{+\bullet}H_BQ_B^{-\bullet}(d)^U$ has a higher energy. Conversion to the final relaxed $D^{+\bullet}H_BQ_B^{-\bullet}(p)^R$ occurs at room temperature but is impaired at low temperatures (*e.g.* 80K). The slower charge recombination from the relaxed state $k_{BD}{}^R << k_{BD}{}^U$ is attributed to charge stabilization due to protein and water relaxation.

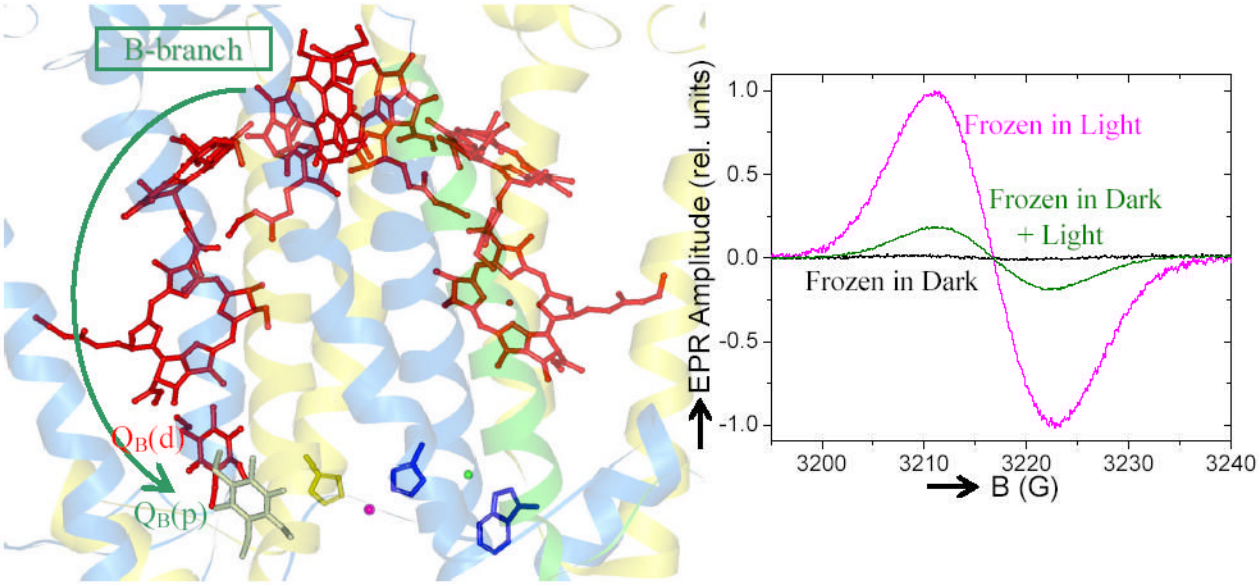

Table 1

Summary of amplitudes and quantum efficiencies of quinone reduction in native and B-branch mutant RCs (Eqns. 3 and 4)

Sample	A(1)	Φ(1)	A(2)	Φ(2)	A(3)	Φ(3)	τ (s)[1]
Native[2]	0.95	100%	.05	~1%	--	--	.033, 6
AWM260	0.69	n.d.	.31	0.2%	--	--	6
LHM214/AWM260	0.71	n.d.	.29	0.2%	--	--	6
GDM203AWM260	0.70	n.d.	.30	0.2%	--	--	6
FYL181/LHM214/ AWM260	0.71	n.d.	.19	0.3%	.10	20%	6
FYL181/GDM203/ YFM210/LHM214/ AWM260 (Quintuple)	0.71	n.d.	.20	0.3%	.09	20%	6

--, not applicable; n.d., could not be determined from the data since charge separated state was not stably formed in this fraction of the population. The statistical error in the estimated values is ~20%, but there is also an expected systematic error of ~20% introduced by the assumption that the cross section is identical in the samples. Thus, the estimates are accurate to approximately a factor of 2.

[1] This is the average time constant for decay back to the ground state; in general the recombination kinetics are multiphasic.

[2] The quantum efficiency is for forming $D^+Q_A^-$ (φ_A) and was taken to be 1.0 (*i.e.* 100%) for the Native RC with a lifetime of 30ms. The quantum efficiency for forming the more stable phase is ~1% with a lifetime of 6s. A more detailed analysis and discussion is presented elsewhere (60).